treme and prolonged environmental stress (*39*) and were likely unaffected. Many eukaryotic phyla (including red, green, and chromophytic algae) evolved before the late Neoproterozoic glaciations and also must have survived the environmental stress (*40*). However, a succession of snowball glaciations must have imposed an intense environmental filter, resulting in a series of genetic "bottleneck and flush" cycles (*41*), possibly leading to an initial metazoan radiation before the terminal glaciation (*42*) and an Ediacaran radiation in its aftermath (*11*).

References and Notes

1. A. H. Knoll, *Sci. Am.* **265**, 64 (October 1991); _____ and M. R. Walter, *Nature* **356**, 673 (1992); A. H. Knoll, in *Origin and Evolution of the Metazoa*, J. H. Lipps and P. W. Signor, Eds. (Plenum, New York, 1992), pp. 53–84.
2. G. C. Bond, P. A. Nickeson, M. A. Kominz, *Earth Planet. Sci. Lett.* **70**, 325 (1984); P. F. Hoffman, *Science* **252**, 1409 (1991); I. W. D. Dalziel, *Annu. Rev. Earth Planet. Sci.* **20**, 501 (1992); C. M. Powell, Z. X. Li, M. W. McElhinny, J. G. Meert, G. K. Park, *Geology* **21**, 889 (1993); A. B. Weil, R. Van der Voo, C. Mac Niocall, J. G. Meert, *Earth Planet. Sci. Lett.* **154**, 13 (1998).
3. W. B. Harland, *Geol. Rundsch.* **54**, 45 (1964).
4. M. J. Hambrey and W. B. Harland, *Earth's Pre-Pleistocene Glacial Record* (Cambridge Univ. Press, Cambridge, 1981).
5. G. M. Young, *Geology* **23**, 153 (1995).
6. J. D. Roberts, *J. Geol.* **84**, 47 (1974); J. D. Aitken, *Bull. Geol. Surv. Can.* **404**, 1 (1991); I. J. Fairchild, in *Sedimentology Review 1*, V. P. Wright, Ed. (Blackwell, Oxford, 1993), pp. 1–16.
7. M. J. Kennedy, *J. Sediment. Res.* **66**, 1050 (1996).
8. Although Phanerozoic cool-water skeletal carbonates are not uncommon [N. P. James and J. A. D. Clarke, *Cool-Water Carbonates* (Society for Sedimentary Geology, Tulsa, OK, 1997)], the inverse solubility of $CaCO_3$ with temperature mitigates against such an origin for inorganic carbonates with abundant aragonitic sea-floor cements, which are typical of Neoproterozoic postglacial cap carbonates [T. M. Peryt *et al.*, *Sedimentology* **37**, 279 (1990); (*7*)].
9. H. Martin, *The Precambrian Geology of South West Africa and Namaqualand* (Precambrian Research Unit, University of Cape Town, Cape Town, South Africa, 1965); J. V. N. Dorr Jr., *Econ. Geol.* **68**, 1005 (1973); G. M. Young, *Precambrian Res.* **3**, 137 (1976).
10. A. H. Knoll, J. M. Hayes, A. J. Kaufman, K. Swett, I. B. Lambert, *Nature* **321**, 832 (1986); A. J. Kaufman, J. M. Hayes, A. H. Knoll, G. J. B. Germs, *Precambrian Res.* **49**, 301 (1991); A. J. Kaufman and A. H. Knoll, *ibid.* **73**, 27 (1995). The carbon isotopic compositions of carbonates were determined according to procedures described in these references and in (*11*) and were reported as $\delta^{13}C$ values relative to Vienna Pee Dee belemnite in units per mil defined as $[(R_{sample}/R_{standard}) - 1] \times 10^3$, where $R = {}^{13}C/{}^{12}C$.
11. A. J. Kaufman, A. H. Knoll, G. M. Narbonne, *Proc. Natl. Acad. Sci. U.S.A.* **94**, 6600 (1997).
12. R. Buick, D. J. Des Marais, A. H. Knoll, *Chem. Geol.* **123**, 153 (1995); L. C. Kah and J. K. Bartley, *Geol. Soc. Am. Abstr. Programs* **29**, 115 (1997); M. D. Brasier and J. F. Lindsay, *Geology* **26**, 555 (1998).
13. W. T. Holser, in *Patterns of Change in Earth Evolution*, H. D. Holland and A. F. Trendall, Eds. (Springer-Verlag, Berlin, 1984), pp. 123–143.
14. P. W. Schmidt and G. E. Williams, *Earth Planet. Sci. Lett.* **134**, 107 (1995); L. E. Sohl, *Geol. Soc. Am. Abstr. Programs* **29**, 195 (1997); J. K. Park, *Can. J. Earth Sci.* **34**, 34 (1997).
15. P. F. Hoffman, A. J. Kaufman, G. P. Halverson, *GSA Today* **8**(5), 1 (1998).
16. M. R. Rampino, *J. Geol.* **102**, 439 (1994); G. E. Williams, *Geol. Mag.* **112**, 441 (1975); *Earth Sci. Rev.* **34**, 1 (1993).
17. J. L. Kirschvink [in *The Proterozoic Biosphere*, J. W. Schopf and C. Klein, Eds. (Cambridge Univ. Press, New York, 1992), pp. 51–52] extended an idea originally proposed by W. B. Harland (*3*).
18. R. M. Miller, in *African Basins*, vol. 3 of *Sedimentary Basins of the World*, R. C. Selley, Ed. (Elsevier, Amsterdam, 1997), pp. 237–268.
19. K. H. Hoffmann and A. R. Prave, *Communs. Geol. Surv. Namibia* **11**, 47 (1996).
20. J. G. Meert, R. Van der Voo, S. Ayub, *Precambrian Res.* **74**, 225 (1995); J. G. Meert and R. Van der Voo, *J. Geol.* **104**, 131 (1996).
21. Discussions of diagenesis in Neoproterozoic carbonates and descriptions of methods for screening samples before isotopic analysis are contained in (*10*) and (*11*).
22. M. J. Kennedy, A. R. Prave, K. H. Hoffmann, *Geol. Soc. Am. Abstr. Programs* **29**, 196 (1997).
23. L. R. Kump, *Geology* **19**, 299 (1991).
24. D. J. Des Marais and J. G. Moore, *Earth Planet. Sci. Lett.* **69**, 43 (1984).
25. K. Caldeira and J. F. Kasting, *Nature* **359**, 226 (1992). The time required to achieve meltback would be less if the ice surface became darkened by volcanic ash. However, the effect of ash accumulation would be countered by hoarfrost formation that originated from volcanic outgassed H_2O. Caldeira and Kasting reported the possibility of irreversible icehouse conditions due to the formation of CO_2 clouds, as did Kirschvink (*17*), but it now appears that cooling actually may be limited by CO_2 clouds [F. Forget and R. T. Pierrehumbert, *Science* **278**, 1273 (1997)].
26. S. N. Williams, S. J. Schaefer, V. Calvache, M. D. Lopez, *Geochim. Cosmochim. Acta* **36**, 1765 (1992).
27. K. Caldeira, *Geology* **19**, 204 (1991).
28. H. Elderfield and A. Schultz, *Annu. Rev. Earth Planet. Sci.* **24**, 191 (1996); R. E. McDuff and J. M. Gieskes, *Earth Planet. Sci. Lett.* **33**, 1 (1976).
29. J. W. Morse and M. L. Bender, *Chem. Geol.* **82**, 265 (1990).
30. Sea-floor crystal fans, pseudomorphic after aragonite (not ikaite) and reeflike in overall construction, occur locally in the Maieberg cap carbonate (G. Soffer, personal communication).
31. Analysis of tidal rhythmites indicates ~400 solar days in the late Neoproterozoic year [G. E. Williams, *J. Phys. Earth* **38**, 475 (1990); C. P. Sonett, E. P. Kvale, A. Zakharian, M. A. Chan, T. M. Demko, *Science* **273**, 100 (1996)].
32. J. P. Grotzinger and A. H. Knoll, *Palaios* **10**, 578 (1995); A. H. Knoll, R. K. Bambach, D. E. Canfield, J. P. Grotzinger, *Science* **273**, 452 (1996).
33. H. G. Marshall, J. C. G. Walker, W. R. Kuhn, *J. Geophys. Res.* **93**, 791 (1988); W. W. Hay, E. J. Barron, S. L. Thompson, *J. Geol. Soc. London* **147**, 749 (1990); T. J. Crowley and S. K. Baum, *J. Geophys. Res.* **98**, 16723 (1993).
34. J. I. Hedges and R. G. Keil, *Mar. Chem.* **49**, 81 (1995).
35. V. A. Melezhik and A. E. Fallick, *Mineral. Mag.* **58A**, 593 (1994); D. A. Evans, N. J. Beukes, J. L. Kirschvink, *Nature* **386**, 262 (1997).
36. P. Van Cappellen and E. D. Ingall, *Paleoceanography* **9**, 677 (1994).
37. D. E. Canfield and A. Teske, *Nature* **382**, 127 (1996); S. J. Carpenter and K. C. Lohmann, *Geochim. Cosmochim. Acta* **61**, 4831 (1997).
38. G. Vidal and M. Moczydlowska-Vidal, *Paleobiology* **23**, 230 (1997); A. H. Knoll, *Proc. Natl. Acad. Sci. U.S.A.* **91**, 6743 (1994).
39. W. J. Green and E. I. Friedmann, Eds., *Physical and Biogeochemical Processes in Antarctic Lakes*, vol. 59 of *Antarctic Research Series* (American Geophysical Union, Washington, DC, 1993); K. H. Nealson, *J. Geophys. Res.* **102**, 23675 (1997).
40. A. H. Knoll, *Science* **256**, 622 (1992).
41. H. L. Carson, *Annu. Rev. Genet.* **21**, 405 (1987); K. J. Niklas, *The Evolutionary Biology of Plants* (Univ. of Chicago Press, Chicago, 1997).
42. H. J. Hofmann, G. M. Narbonne, J. D. Aitken, *Geology* **18**, 1199 (1990).

43. We thank S. Bowring, J. Edmond, B. Farrell, M. Delaney, J. Grotzinger, A. Knoll, J. Marshall, M. McElroy, and P. Myrow for discussions. B. Holtzman, G. Hu, A. Maloof, A. Prave, G. Soffer, and D. Sumner contributed to fieldwork. The manuscript benefited from comments by K. Caldeira, L. Derry, D. Erwin, L. Kump, and an anonymous reviewer. This work was supported by NSF grants EAR 95-06769, EAR 95-10339, EAR 96-30928, EAR 96-14070, and OCE 97-33688; the National Sciences and Engineering Research Council of Canada; the Canadian Institute of Advanced Research; Harvard University; the University of Maryland; and the Geological Survey of Namibia.

21 April 1998; accepted 21 July 1998

Photofragment Helicity Caused by Matter-Wave Interference from Multiple Dissociative States

T. Peter Rakitzis, S. Alex Kandel, Andrew J. Alexander, Zee Hwan Kim, Richard N. Zare*

Isolated diatomic molecules of iodine monochloride (ICl) were photodissociated by a beam of linearly polarized light, and the resulting ground-state Cl atom photofragments were detected by a method that is sensitive to the handedness (helicity) of the electronic angular momentum. It was found that this helicity oscillates between "topspin" and "backspin" as a function of the wavelength of the dissociating light. The helicity originates solely from the (de Broglie) matter-wave interference of multiple dissociating pathways of the electronic excited states of ICl. These measurements can be related to the identity and to the detailed shapes of the dissociating pathways, thus demonstrating that it is possible to probe repulsive states by spectroscopic means.

The photodissociation of a diatomic molecule occurs, in the simplest case, as the breakup of an excited molecule on a single potential energy surface (*1*). The molecule then dissociates under the influence of a force directed along the bond axis. The photodissociation

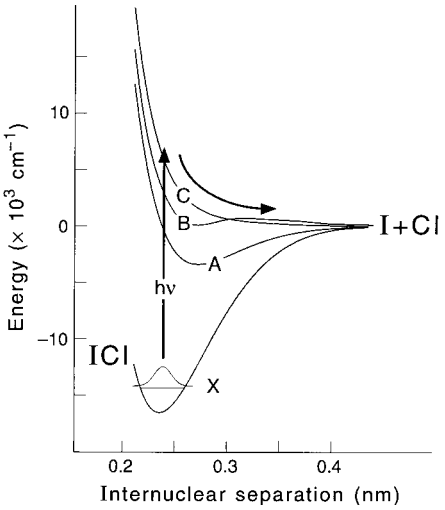

Fig. 1. Potential energy curves as a function of the internuclear separation for the ground electronic state (labeled X) and the three lowest excited electronic states (labeled A, B, and C) of ICl. At large internuclear separations, all three excited-state curves correlate to ground-state I and Cl atoms. The absorption of linearly polarized light in the range of 490 to 560 nm ($h\nu$ is the energy of a photon) causes ICl to dissociate to I and Cl atoms via the three dissociative pathways, indicated by a curved arrow. Interference between the $\Omega' = 0$ (B state) and $\Omega' = 1$ pathways (A and C states) produces I and Cl atoms with oriented angular momenta (with topspin or backspin).

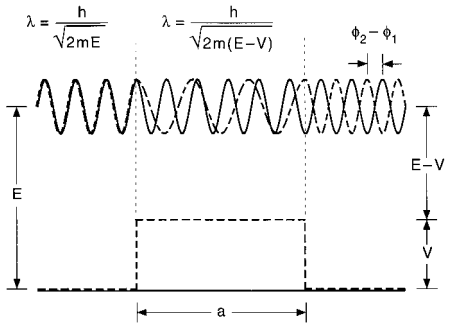

Fig. 2. Development of the asymptotic phase shift, $(\varphi_2 - \varphi_1)$, between two matter waves of energy E, one of which follows a flat potential (solid), and the other of which encounters an energy barrier of height V and width a (dashed). The de Broglie wavelength is a function of E, V, the mass, m, and Planck's constant, h. Note that the two matter waves have different wavelengths only above the barrier.

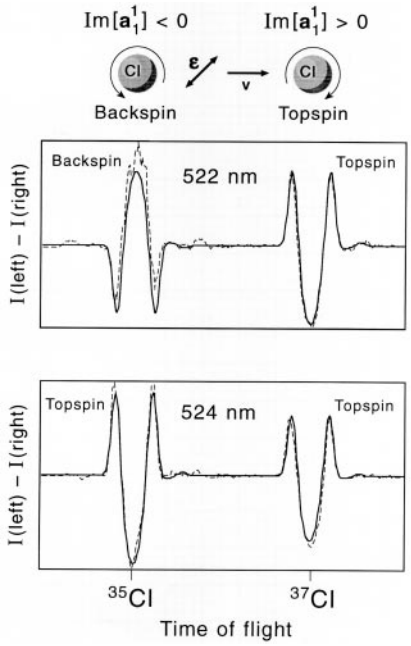

Fig. 3. Experimental time-of-flight difference profiles for ^{35}Cl and ^{37}Cl atoms {left minus right circularly polarized light [I(left) and I(right), respectively]}. The profiles are centered at arrival times of 4.80 and 4.94 μs, respectively. These difference profiles have a characteristic shape, and their size is proportional to $Im[\mathbf{a}_1^1]$ (photofragment helicity). The motions of topspin and backspin are defined with respect to the Cl-atom velocity, **v**, and the electric vector of the dissociating light, $\boldsymbol{\varepsilon}_{phot}$, as shown. A positive $Im[\mathbf{a}_1^1]$ value describes angular momenta pointing preferentially into the page, corresponding to a motion with topspin (with respect to the vectors $\boldsymbol{\varepsilon}_{phot}$ and **v**), whereas a negative $Im[\mathbf{a}_1^1]$ value describes angular momenta pointing preferentially out of the page, corresponding to a motion with backspin.

products are often open-shell atoms with electronic angular momenta. In single-surface photodissociations with linearly polarized light, the symmetry of the dissociation process constrains the electronic angular momentum of the atomic photofragment to lack helicity, that is, "up" is equivalent to "down" and "left" is equivalent to "right." In the more general case, the dissociative transition at a fixed photon energy can prepare more than one excited state, and the molecule can break apart on several potential energy surfaces simultaneously. Quantum interference between multiple electronic pathways in the dissociation has been analyzed theoretically (*2–5*), and it has been shown that it can lead to helicity in the angular momenta of the atomic fragments (*6*). We report an experimental observation of this effect in the photodissociation of ICl and demonstrate how interference effects in molecular dissociation cause helicity of the photofragment angular momenta, which vary in an oscillatory fashion with photolysis energy. This oscillation of electronic helicity depends sensitively on the shapes of the interfering potential energy curves. Just as interference in x-ray diffraction is used to deduce molecular structure, we demonstrate how interference in photodissociation can be used to deduce the shape of molecular excited states. The measurements presented here constitute a spectroscopic method for analyzing repulsive excited-state potentials and permit a rigorous test of the calculation of these potentials.

Electrons in atoms and molecules have two types of angular momentum: the intrinsic electronic spin and electronic orbital angular momentum. In general, the electrons that constitute a chemical bond pair up their spins such that the total spin of the molecule is zero. Similarly, the total electronic orbital angular momentum usually has no net projection along a bond axis. Therefore, the net projection of the total angular momentum along the bond axis, Ω, is zero for the ground state of most diatomic molecules. The absorption of a single photon can promote the transition of the diatomic molecule from the $^1\Sigma^+$ ($\Omega = 0$) ground state labeled X in Fig. 1, to excited electronic states with $\Omega' = 0$ or $\Omega' = 1$, known as parallel and perpendicular transitions, respectively. For example, ab initio calculations (*7, 8*) have shown that the absorption of green light from the $\Omega = 0$ ground state of ICl leads to two $\Omega' = 1$ excited states (the $^3\Pi_1$ and $^1\Pi_1$ states, labeled as A and C, respectively) through a perpendicular transition, and to one $\Omega' = 0$ excited state (the $^3\Pi_{0+}$ state, labeled as B) through a parallel transition (Fig. 1). Parallel transitions produce photofragments with velocities preferentially parallel to the electric vector, $\boldsymbol{\varepsilon}_{phot}$, of the linearly polarized photolysis light (in a $\cos^2\theta$ distribution, where θ is the angle between $\boldsymbol{\varepsilon}_{phot}$ and the recoil direction), whereas perpendicular transitions produce photofragments with velocities preferentially perpendicular to the electric vector of the linearly polarized photolysis light (in a $\sin^2\theta$ distribution) (*9*). Measurements of the spatial distribution of the photofragment velocities as a function of the dissociating wavelength show that at 490 nm the photodissociation occurs almost entirely through the $\Omega' = 0$ state; at 560 nm the photodissociation occurs almost entirely through one or both of the $\Omega' = 1$ states; and at intermediate wavelengths a mixture of $\Omega' = 0$ and $\Omega' = 1$ states are accessed (*10*). Measurements of the spatial distribution of the photofragments do not allow the determination of the relative contribution of the two $\Omega' = 1$ states.

The origin of photofragment helicity can be explained in classical terms by considering the motion of the charge distribution. For a parallel (or perpendicular) transition, the absorption of a linearly polarized photon causes the charge distribution to oscillate parallel (or perpendicular) to the internuclear axis. Upon separation of the diatomic molecule into its two atomic part-

Department of Chemistry, Stanford University, Stanford, CA 94305–5080, USA.

*To whom correspondence should be addressed. E-mail: zare@stanford.edu

ners, no orientation (helicity) of the electronic angular momentum of the atomic photofragments can occur in either case. In a "mixed transition" involving excitation of both parallel and perpendicular transitions, the electron charge cloud initially oscillates along a line that makes an angle with respect to the internuclear axis. This motion can be decomposed into components parallel and perpendicular to the internuclear axis, oscillating in phase. As the nuclei separate, the frequencies of oscillation of these two components can differ so that they are no longer oscillating in phase. The frequency difference is directly related to the energy difference between the interfering dissociating pathways. At large nuclear separations the energy difference vanishes and the frequencies of oscillation become equal again, but with a possible net phase shift (Fig. 2). Thus, the phase shift causes the electron charge cloud to develop elliptical motion (a phase shift of 90° results in pure circular motion), and the resultant

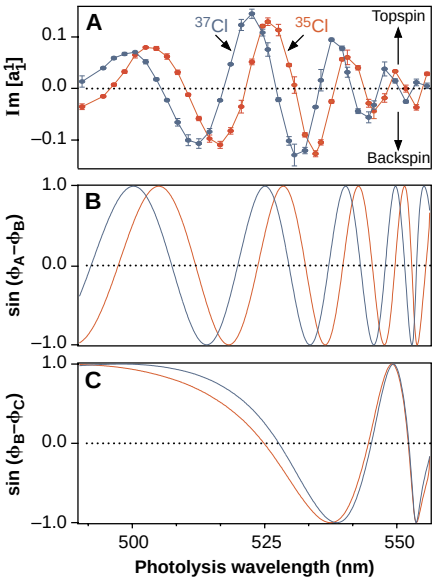

Fig. 4. (**A**) Experimental measurement of the degree of helicity, $Im[\mathbf{a}_1^1]$, of ^{35}Cl and ^{37}Cl from the photolysis of ICl as a function of the wavelength of the dissociating light. The magnitudes of the $Im[\mathbf{a}_1^1]$ parameter have been corrected for the effects of hyperfine depolarization (*24, 25*), and the error bars are statistical (1σ) resulting from replicate measurements. The angular momenta of the Cl atoms oscillate between topspin and backspin as a function of wavelength. (**B**) Calculated de Broglie phase shift $\sin(\varphi_A - \varphi_B)$ as a function of photolysis wavelength for dissociating surfaces A and B, shown in Fig. 1. (**C**) Calculated de Broglie phase shift $\sin(\varphi_B - \varphi_C)$ as a function of photolysis wavelength for dissociating surfaces B and C, shown in Fig. 1. Comparison to experiment shows clearly that the oscillations are matched well by the predicted interference between surfaces A and B, and very poorly by that between B and C.

electronic angular momenta of the atomic photofragments have helicity.

This production of oriented (circularly polarized) matter is analogous to the production of circularly polarized light when linearly polarized light passes through a birefringent crystal, such as a quarter-wave plate (*11*). In the photolysis of ICl, the linearly polarized excitation light (and its associated angular momentum) is separated into components that excite parallel and perpendicular transitions. If a phase difference arises between these components as a result of the energetic differences of the two paths followed by the separating nuclei, then the resulting Cl atoms can have oriented (circularly polarized) angular momenta. The introduction of a phase difference, $(\varphi_2 - \varphi_1)$, between two states separated by a constant potential energy, ΔE, and interacting for a time, t, is well studied in quantum-beat spectroscopy (*12*) and is given by

$$(\varphi_2 - \varphi_1) = \frac{\Delta E t}{\hbar} \qquad (1)$$

where $\hbar$ is Planck's constant divided by 2π. The situation during photodissociation is very similar, except that the instantaneous potential energy difference between the two paths, ΔE, varies as a function of internuclear separation, and an appropriate time integration must be performed to determine the net phase difference.

An equivalent, and more visual, way of calculating the phase difference is to determine the phase shift in the de Broglie waves associated with the nuclear motion along the two paths (Fig. 2). This method is equivalent because the difference in potential energy between the two paths at any instant is equal to the difference in kinetic energy of the atoms at the same instant. The de Broglie wavelength of the chlorine atoms, $\lambda(r)$, as a function of internuclear separation, r, is given by

$$\lambda(r) = \frac{h}{\sqrt{2m[E - V(r)]}} \qquad (2)$$

where E is the total energy, $V(r)$ is the potential energy as a function of internuclear separation, m is the mass of the chlorine atom, and h is Planck's constant. Different energetic pathways can support different numbers of de Broglie wavelengths (Fig. 2), so that a phase difference, $(\varphi_2 - \varphi_1)$, can be introduced into the two wave packets. The degree of helicity is proportional to $\sin(\varphi_2 - \varphi_1)$. Therefore, the determination of the photofragment helicity provides a direct measurement of the phase difference of de Broglie matter waves associated with the multiple dissociating pathways.

Our experimental approach is similar to that reported in (*13*). Briefly, ICl molecules from a pulsed supersonic beam expansion are photolyzed with linearly polarized light in the range of 490 to 560 nm. The resulting ground-state Cl atom photofragments are ionized through absorption of three circularly polarized photons at 235 nm, to produce Cl^+ ions. The absorption of circularly polarized probe light is sensitive to the helicity of the angular momentum of the Cl atoms. The Cl^+ ions are detected with a time-of-flight mass spectrometer, and the width of the time-of-flight profiles (Fig. 3) is sensitive to the recoil velocity of the Cl atoms (*13*). The gross orientation of the electronic angular momenta of the Cl atoms can be described by the single dimensionless parameter $Im[\mathbf{a}_1^1]$ (*2, 13–15*), that in this case lies between $-\sqrt{3/10}$ and $\sqrt{3/10}$. This parameter describes a preference for an orientation of the angular momenta perpendicular to the plane defined by the photolysis laser polarization vector, $\boldsymbol{\varepsilon}_{phot}$, and the Cl atom velocity, $\mathbf{v}$ (Fig. 3).

The time-of-flight signal differences for left and right circularly polarized probe light at photolysis wavelengths of 522 and 524 nm are shown in Fig. 3. At a photolysis wavelength of 524 nm, both Cl isotopes have topspin, whereas at 522 nm, the ^{35}Cl photofragments have backspin and the ^{37}Cl photofragments have topspin (*16*). Similar measurements were performed in the 490- to 560-nm region, allowing the determination of the photofragment helicity, $Im[\mathbf{a}_1^1]$, as a function of photolysis wavelength for both Cl isotopes (Fig. 4A). In this wavelength region, the photolysis of ICl yields oriented Cl atoms that oscillate rapidly between topspin and backspin as a function of photolysis wavelength. This interference pattern represents a direct measurement of the phase difference of de Broglie wavelengths from the matter waves associated with multiple dissociating paths. The mass effect evident from the difference between the curves for ^{35}Cl and ^{37}Cl (Fig. 4A) arises from the mass dependence of the de Broglie wavelength shown in Eq. 2. Photolysis wavelength–dependent oscillations caused by coherence effects are discussed in the work of Siebbeles and Beswick (*4*). Note that the experimental oscillation pattern has an envelope that decays at both long and short wavelengths. The magnitude of the interference is greatest when the contributions from the $\Omega' = 0$ and $\Omega' = 1$ surfaces are equal, but tends toward zero when the contribution from either the $\Omega' = 0$ or $\Omega' = 1$ surface dominates. Spatial photofragment distribution measurements (*10*) have shown that the contributions from the $\Omega' = 0$ and $\Omega' = 1$ surfaces are equal at about 525 nm and diverge at both shorter and longer wavelengths. This behavior predicts an envelope for the oscillation of the orientation that peaks at 525 nm, in agreement with that observed. However, the spatial distribution measurements are not accurate enough to pre-

dict the precise shape of the envelope, so we cannot rule out other factors contributing to the envelope shape.

We have solved numerically the one-dimensional Schrödinger equation for surfaces A, B, and C as a function of the dissociation energy to determine the energy-dependent phase differences, $(\varphi_A - \varphi_B)$ and $(\varphi_B - \varphi_C)$, in analogy to the simple example shown in Fig. 2. The photofragment orientation, $Im[\mathbf{a}_1^1]$, is linearly proportional to $\sin(\varphi_A - \varphi_B)$ and $\sin(\varphi_B - \varphi_C)$. Comparison of the photodissociation-wavelength dependence of these functions (Fig. 4, B and C) to experiment shows that the interference pattern is caused predominantly from dissociation via surfaces A and B. Overall, we conclude that at a photolysis wavelength of 490 nm, ICl dissociates predominantly via the B state; at 560 nm, ICl dissociates predominantly via the A state; and at intermediate wavelengths, the dissociation proceeds coherently through both states. The oscillations of $\sin(\varphi_A - \varphi_B)$ shown in Fig. 4B match very well the experimental oscillations in Fig. 4A, in contrast to the calculations shown in Fig. 4C. We conclude that the C state does not significantly participate in the photodissociation. The match at short wavelengths between Figs. 4A and 4B indicates that the calculated surfaces A and B are quite accurate; however, at longer wavelengths the calculated oscillations of $\sin(\varphi_A - \varphi_B)$ are too rapid. We suggest that this discrepancy may indicate that the shapes of the surfaces A and B need to be slightly improved.

To our knowledge, this study represents the first observation that the photolysis of a molecule with linearly polarized light causes the production of oriented photofragments. Previously, oriented photofragments have been observed using photolysis with circularly polarized light (*17–22*), but such orientation does not necessarily arise from matter-wave interference. This technique is not limited to diatomic molecules (*23*) and can be used to study excited states and dissociative processes with unprecedented sensitivity. Conventional spectroscopy is sensitive to the shape and nature of bound electronic states. In contrast, the interference pattern of the photofragment orientation is sensitive to the shape and nature of dissociating states. This technique can be used to investigate the unimolecular decomposition of chemical systems involving multiple electronic states by coherently preparing more than one electronic state of different symmetry. As such, the technique may become an important probe of wave-packet dynamics on multiple dissociative surfaces.

References and Notes

1. R. Schinke, *Photodissociation Dynamics: Molecular Motion in Excited States* (Wiley, New York, 1992).
2. L. D. A. Siebbeles, M. Glass-Maujean, O. S. Vasyutinskii, J. A. Beswick, O. Roncero, *J. Chem. Phys.* **100**, 3610 (1994).
3. O. S. Vasyutinskii, *Sov. Phys. JETP* **54**, 855 (1981).
4. L. D. A. Siebbeles and J. A. Beswick, *J. Chem. Soc. Faraday Trans.* **88**, 2565 (1992).
5. M. Glass-Maujean and J. A. Beswick, *Phys. Rev. A* **36**, 1170 (1987).
6. In the celebrated Young's two-slit experiment, the interference of light passing through two slits causes a bright and dark fringe pattern to appear on a screen, the intensity of which varies as $\cos\Delta\phi$ (where $\Delta\phi$ is the phase difference between the two paths). If instead, the light used is initially linearly polarized, and crossed polarizers are placed in front of the two slits (at 45° to the linear polarization so that both slits transmit equally), then the light on the screen no longer shows an intensity fringe pattern, but shows instead a polarization fringe pattern. This polarization pattern can be separated into components with linearly polarized variations (proportional to $\cos\Delta\phi$) and circularly polarized variations (proportional to $\sin\Delta\phi$). The analog of this special two-slit experiment in molecular photolysis is that in which the interference of matter waves from potential surfaces of different symmetry causes angular momentum polarization of the photofragments [for discussions and examples of $\cos\Delta\phi$ variations in the alignment of photofragments, see E. Flemming, O. Wilhelmi, H. Schmoranzer, M. Glass-Maujean, *J. Chem. Phys.* **103**, 4090 (1995) and (*4, 5, 25*)]. The experiment described in the present report is an example of the $\sin\Delta\phi$ variations in photofragment helicity.
7. We thank S. Yabushita for permission to use his ab initio calculations of the excited states of ICl.
8. K. Tonokura *et al*., *J. Chem. Phys.* **99**, 3461 (1993).
9. R. N. Zare and D. R. Herschbach, *Proc. IEEE* **51**, 173 (1963).
10. T. P. Rakitzis, S. A. Kandel, A. J. Alexander, Z. H. Kim, R. N. Zare, unpublished results.
11. In such crystals, the wavelength and speed of light that is linearly polarized parallel to the optical axis of the crystal differs from that which is linearly polarized perpendicular to the optical axis. Light that is polarized at some angle (such as 45°) to the optical axis has components that are parallel and perpendicular to the optical axis. These components, which were in phase upon entering the crystal, change phase as the light propagates through the crystal. A phase difference of a quarter wave upon exiting the crystal produces pure circularly polarized light.
12. E. Hack and J. R. Huber, *Int. Rev. Phys. Chem.* **10**, 287 (1991).
13. T. P. Rakitzis, S. A. Kandel, R. N. Zare, *J. Chem. Phys.* **107**, 9382 (1997).
14. T. P. Rakitzis and R. N. Zare, unpublished results.
15. A. J. Orr-Ewing and R. N. Zare, *Annu. Rev. Phys. Chem.* **45**, 315 (1994).
16. The combined system of uniformly distributed ICl molecules and a beam of linearly polarized light has no net helicity; therefore, no net helicity can appear after photolysis. In the axial recoil approximation, no angular momentum appears in the translational motion of the photofragments, and the helicity of the Cl atoms must be exactly counterbalanced by an opposite helicity of the I atoms. Therefore, unless the I atoms from $I^{35}Cl$ and $I^{37}Cl$ can be distinguished, the orientation of the I atoms will reflect the 3:1 population-weighted sum of the ^{35}Cl and ^{37}Cl orientations and reflect similar information.
17. O. S. Vasyutinskii, *Opt. Spectrosc.* (*USSR*) **51**, 124 (1980).
18. D. V. Kupriyanov, B. V. Picheyev, O. S. Vasyutinskii, *J. Phys. B* **26**, L803 (1993).
19. D. V. Kupriyanov and O. S. Vasyutinskii, *Chem. Phys.* **171**, 25 (1993).
20. D. V. Kupriyanov, B. N. Sevastianov, O. S. Vasyutinskii, *Z. Phys. D* **15**, 105 (1990).
21. E. Hasselbrink, J. R. Waldeck, R. N. Zare, *Chem. Phys.* **126**, 191 (1988).
22. J. F. Black, E. Hasselbrink, J. R. Waldeck, R. N. Zare, *Mol. Phys.* **71**, 1143 (1990).
23. For the photolysis of polyatomic systems, photofragment helicity should be detectable under the following conditions: one photofragment is detected in a state-specific manner, and its velocity distribution is detected with an energy resolution greater than the internal energy spacings of the undetected fragment. For poorer energy resolution, some reduction in the photofragment helicity is expected but may not be severe, depending on how rapidly the photofragment helicity varies with the internal state of the undetected photofragment.
24. A. J. Orr-Ewing, W. R. Simpson, T. P. Rakitzis, R. N. Zare, *Isr. J. Chem.* **34**, 95 (1994).
25. T. P. Rakitzis, S. A. Kandel, R. N. Zare, *J. Chem. Phys.* **108**, 8291 (1998).

26. Support from the NSF under grant number CHE-93-22690 is gratefully acknowledged.

22 May 1998; accepted 22 July 1998

Reversal of Phencyclidine Effects by a Group II Metabotropic Glutamate Receptor Agonist in Rats

Bita Moghaddam* and Barbara W. Adams

Glutamatergic abnormalities have been associated with several psychiatric disorders, including schizophrenia and addiction. Group II metabotropic glutamate receptors were targeted to normalize glutamatergic disruptions associated with an animal model of schizophrenia, the phencyclidine model. An agonist of this group of receptors, at a dose that was without effects on spontaneous activity and corticolimbic dopamine neurotransmission, attenuated the disruptive effects of phencyclidine on working memory, stereotypy, locomotion, and cortical glutamate efflux. This behavioral reversal occurred in spite of sustained dopamine hyperactivity. Thus, targeting this group of receptors may present a nondopaminergic therapeutic strategy for treatment of psychiatric disorders.

Several lines of evidence suggest that glutamatergic mechanisms contribute to the pathophysiology of schizophrenia (*1–3*). For example, phencyclidine (PCP) and other antagonists of *N*-methyl-D-aspartate (NMDA) receptors have psychotomimetic

Photofragment Helicity Caused by Matter-Wave Interference from Multiple Dissociative States

T. Peter Rakitzis *et al.*

Science **281**, 1346 (1998);
DOI: 10.1126/science.281.5381.1346

Science (print ISSN 0036-8075; online ISSN 1095-9203) is published weekly, except the last week in December, by the American Association for the Advancement of Science, 1200 New York Avenue NW, Washington, DC 20005.